A Hybrid EA Approach to Multisensor Image Superresolution

A Hybrid EA Approach to Multisensor Image Superresolution+

Noel Mendoza*, Yen-Wei Chen**, and Zensho Nakao**

Email:{nmendoza, chen}@augusta.eee.u-ryukyu.ac.jp

Abstract

This paper considers the problem of reconstructing a high-resolution image from multiple under-sampled, shifted and noisy low-resolution frames. Using a hybrid evolutionary algorithm we attempt to reconstruct the original high-resolution image from a sequence of images corresponding to the same scene but shifted by unknown values in both scalar directions and degraded by Gaussian artifacts. The algorithm is easy to implement and can exploit subtle subpixel variations. It can obtain lossy, much more acceptable results than ordinary interpolation. This is exemplified by comparing results with those obtained through conventional interpolation.

Keywords: superresolution, stochastic relaxation, hybrid EA, concurrent simplex, image restoration, interpolation kernels

1 Introduction.

Many image processing applications, such as satellite, medical and scientific imaging require high resolution detailed images. However, physical constraints limit image resolution quality. Current imaging systems yield aliased and under-sampled images This is particularly true for infrared images and some charged coupled device cameras(CCD) whose detectors are not sufficiently dense. Although CCD cameras of more than 2 million pixels have been developed, there is still a need to increase the resolution further. Reducing the size of the pixels(photo-detectors) is one obvious way. But since decreasing the size of the pixels also lessens the amount of light available for each detector, the overall picture quality is degraded[1,2,7]. The existence of shot-noise (variation of input) is unavoidable. Inasmuch as sensor modification exacts tremendous effort and expense, attention has turned to the use of numerical techniques to obtain higher resolution images[3].

Superresolution attempts to produce a high-resolution image from under-sampled, shifted, degraded images. The reconstructed high-resolution image is not only visually pleasing, but can be of aid to subsequent image processing tasks such as image segmentation and recognition. The use of more than one frame facilitate the efficient determination of high frequency details, which ordinary interpolation can not.

Superresolution is typically a two step process involving image registration and reconstruction[4]. When frame displacements are uncontrolled and consequently, unknown, the low resolution frames usually do not coincide exactly. The displacement of a frame relative to a chosen reference frame has to be measured by some image registration process.

The next phase, i.e. image reconstruction, commences after registration with the aim of obtaining a higher resolution image by combining low-resolution frames and minimizing degradation. However, the presence of unwanted artifacts such as noise as well as registration errors due to aliased frequency components in the low resolution images account for the poor quality of superresolved images.

Superresolution is an ill-conditioned and typically underdetermined large-scale problem involving thousands of unknowns. For example, a total of 200x200=40000 unknown pixels in the high-resolution image is required in superresolving a sequence of 100x100 pixels by a factor of 2 in each spatial direction. The problem's ill-posed nature exacerbates blurring and noise effects. Although, due to practical and theoretical importance, the reconstruction of high resolution images have been studied extensively, some do not adequately address computational and numerical issues[5].

Previous researches have shown that superresolution can be recast as a twin optimization problem. By minimizing the difference between estimated and given low resolution images, not only can the original high resolution frame be obtained but the relative displacements of the low resolution frames as well. In this paper we present a evolutionary hybrid approach to multisensor image superresolution. The algorithm is superior to interpolation methods and poses as a good match for the a modified Stochastic Relaxation method[4] presented previously.

More of said method will be explained in Section 4. The multi-sensor image degradation model is conceptualized in Section 2. Section 3 presents more of the problem. Section 5 talks about the experiment and presents results. A brief summary follows.

2 Image Degradation Model

Conceptually, superresolution, multi-channel, and multi-sensor data fusion are very similar problems. Quite a number of problem models exist [5]. For sake of simplicity we chose to adopt a similar version of multi-sensor model presented by Boo et al[6], shown below, and described as

受理:２０００年１２月２５日

+本論文の一部は平成 12 年度電気学会・電子情報通信学会合同講演会で発表済み

*理工学研究科電気電子工学専攻

**工学部電気電子工学科

follows:

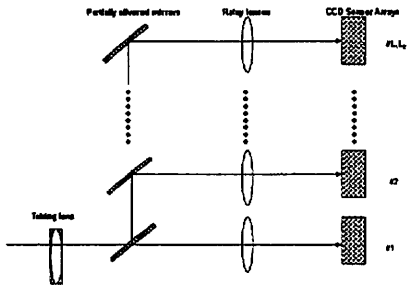

Fig. 1 Image formation systems of Bose et al using multiple CCD sensor arrays

Consider an image formation system composed of a set of identical CCD sensor arrays to obtain multiple observed images. Incoming light from the taking lens is split into multiple parts by partially silvered mirrors and passed through the relay lenses before projection onto the set of CCD sensor array where each array produces a single discrete under-sampled image. Shifted under-sampled versions can be obtained by varying the physical locations of the CCD sensors

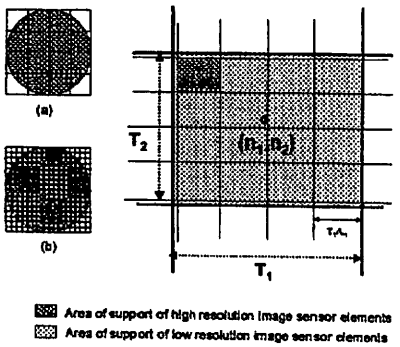

Fig. 2 Area of support for high and low image sensors; (a) low resolution image sensors and (b) high resolution image sensors

determine the sampling positions of the sampled images.

The size of the set of CCD image sensor arrays depends on the decimation ratio between the high and low resolution images (Figure 2). Assuming that each of the sensor arrays consists of N_1xN_2 sensing elements of size $T_1 x\ T_2$. Each sensor array will produce a $N_1\ x\ N_2$ discrete image with the 2D rectangularly shaped interval $T_1 x\ T_2$. If the minimum size of CCD image sensor array is $L_1 x\ L_2$, the original high- resolution image can be discretized at the 2D rectangularly sampled base interval $T_1/L_1 x\ T_2/L_2$. Given this the size of the reconstructed high resolution image is given as M_1xM_2 where $M_1=L_1xN_1$ and $M_2=L_2xN_2$.

Since the physical locations of the CCD sensor arrays determine the sampling positions of the observed under-sampled images, reconstruction of the high-resolution image becomes ill-posed if the CCD image sensor arrays are shifted from each other in both scalar directions. For this experiment, we assume the case that the CCD sensor arrays are shifted from each other by an exact subpixel displacement described by the rectangularly shaped base interval $T_1/L_1 x\ T_2/L_2$. Each of the observed under-sampled images are shifted, down-sampled versions of the high-resolution image. Thus, for $l_1=0,1,\ldots,L_1-1$ and $l_2=0,1,\ldots,L_2-1$ with $[l_1,l_2]\neq 0$, the exact horizontal and vertical displacements of the $[l_1,l_2]$th sensor array with respect to the [0,0]th sensor array are:

$$\delta_{l_1} = \frac{T_1}{L_1} l_1 \qquad \delta_{l_2} = \frac{T_2}{L_2} l_2$$

For $n_1=1,2,\ldots,N_1$ and $n_2=1,2,\ldots,N_2$, the $[l_1,l_2]$th observed undersampled shifted image can be given as:

$$f_{l_1,l_2}[n_1,n_2] = \int_{T_1(n_1-\frac{1}{2})+\delta_{l_1}}^{T_1(n_1+\frac{1}{2})+\delta_{l_1}} \int_{T_2(n_2-\frac{1}{2})+\delta_{l_2}}^{T_2(n_2+\frac{1}{2})+\delta_{l_2}} f_h(x_1,x_2)dx_1dx_2 + v_{l_1,l_2}[n_1,n_2]$$

Where $f_h[x_1,x_2]$ is the continuous bandlimited high-resolution image scene and $v_{l_1,l_2}[n_1,n_2]$ represents the additive discretized noise in the $[l_1,l_2]$th sensor.

The continuous model can be discretized into:

$$f_{l_1,l_2}[m_1,m_2] = \sum_{i_1}\sum_{i_2} h(i_1,i_2;m_1,m_2) \oplus f_h[i_1,i_2] + v_{l_1,l_2}[m_1,m_2]$$

where $f_{l_1,l_2}[m_1,m_2], v_{l_1,l_2}[m_1,m_2]$ represent the $[l_1,l_2]$th low resolution image and noise arrays, and $h(w,x,y,z)$ represent the space-variant point spread function(PSF), which determines the relationship between high and low resolution images.

The discrete under-sampled, low resolution image model $f_{l_1,l_2}[n_1,n_2]$ can be represented in vector form as follows:

Let f_{l_1,l_2}, v_{l_1,l_2} be respectively the (N_1N_2 x 1) observed low resolution image and noise column vectors and let f_h be the desired (M_1M_2 x1) high resolution image. Let

$$D_{l_1} = I_{N_1} \otimes e_{l_1}^t, \qquad D_{l_2} = I_{N_2} \otimes e_{l_2}^t$$

be the 1D vertical and horizontal down-sampling matrices. 1D down-sampling is defined as the Knocker product of (N_1,N_2) the identity matrix I_{N_1}, and the transpose of e_{l_1}, which is the (L_1 x 1) unit vector whose nonzero element is in the l_1th position.

For each sensor, the discrete low resolution image model can be written as:

$$f_{l_1,l_2} = D_{l_1,l_2} H_{l_1,l_2} f_h + v_{l_1,l_2},$$

where H_{l_1,l_2}, $l_1=0,1,\ldots,L_1-1$ and $l_2=0,1,\ldots,L_2-1$ is the

($M_1M_2 \times M_1M_2$) Block Toeplitz-Toeplitz Block(BTTB) blur matrix, and $D_{t_1,t_2} = D_{t_1} \otimes D_{t_2}$ denotes the 2D down-sampling matrix. Because of the large-scale nature of the problem, implementing the above linear model requires sparse matrices.

If we consider blur/down-sampling as the convolution of a source image and a space invariant PSF, superresolution (with unknown displacements) is liken to a set of blind deconvolution operations.

3 Superresolution as an Optimization Problem

If the relative displacements and the down-sampling operation are known, several low-resolution frames can easily be obtained from an estimated high resolution observed image. Superresolution can then be recast as an optimization problem involving the minimization of the difference between said estimated and observed low-resolution images. The estimated and observed low-resolution frames will match only if the estimated high resolution image and the corresponding displacements are correctly determined.

In an attempt to recover both displacements and the original image, we utilized the following cost function:

$$E_{new} = \left\| g_i - r(f, \delta_x, \delta_y) \right\|^2 + \lambda \left\| \nabla f \right\|^2$$

where :

g_i current low resolution frame being compared.
f current high resolution estimate
$r()$ reduces estimate to obtain an estimated low resolution frame
λ regularization parameter
∇f Laplacian constraint

The Laplacian constraint is employed as a smoothing parameter because of its proven efficacy in heuristic image restoration[9]. The cost function used above is similar in form to the Tikonov-Miller regularized conjugate gradient equation below employed by other researchers in the field[5,3,11].

$$P(f) = \min \left\| g - Af \right\|_2^2 + \lambda^2 \left\| Cf \right\|_2^2$$

where :

g low resolution frame being compared.
f high resolution estimate
A estimate to obtain an estimated low resolution frame
λ regularization parameter
C highpass filter

Both equations consist of two parts: a component that attempts to reconstruct a high resolution image by minimizing the difference between estimated and given low resolution frames and another component that minimizes the difference between a pixel and its neighbors, controlling unwarranted oscillations and noise.

4 Hybrid Evolutionary Algorithm

In recent years, soft computing methods have gained tremendous popularity in the solution of nonlinear, ill-posed and blind problems. From hereon , we present a hybrid multi-parent tri-hybrid evolutionary approach[12] which can exploit the global and local search capabilities of EA and Stochastic Relaxation respectively. We shall briefly describe the operations that came into play. Please refer to a previous paper[12] should a more detailed description be deemed necessary.

4.1 Multi-parent Tri-Hybrid EA

Hybrid evolutionary algorithms were formulated to address the convergence problems of traditional EAs[13,14]. The proper integration of a local operator have been known to speed up convergence and obtain more reliable results. Our real-coded tri-hybrid method integrates the features of a multi-parent EA with the efficiency of Simplex Method and Stochastic Relaxation.

Simplex[15], a local operator, is applied to a portion of the

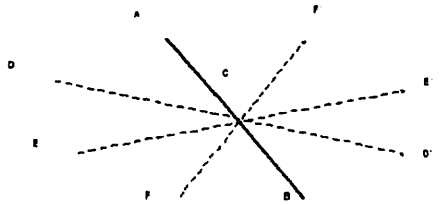

Fig. 3 Two dimensional concurrent simplex

population to further the speed of convergence. A concurrent version of the original method , reflects in lieu of one in lieu of one, p_{n+1}, p_{n+2}, ..., $p_{\Omega-2}$, $p_{n+\Omega}$ points across the centroid(computed from the best N points), to create p'_{n+1}, p'_{n+2}, ..., $p'_{\Omega-2}$, $p'_{n+\Omega}$. All the points are then re-evaluated and a new set of best points (p'_1, p'_2, ..., p'_{n-1}, p'_n) is selected(Fig.2) The reflection operation is determined by the following formula:

$$p_r = p_g + \alpha(p_g - p_{n+1}),$$

α, 's value is set through uniform random distribution. p_r and p_g represent the reflected point and centroid respectively. This approach, termed *Stochastic Simplex*, eases exploration and lets the distance between the centroid and current point to be determined freely.

Stochastic Relaxation, method with foundations in statistical physics, is put to use as a mutation operator. SR was devised to study equilibrium properties of large systems of identical "particles". When combined with an "annealing schedule," SR can be used as a maximization tool as well. It is robust, intrinsically parallel, and very easy to code, in the sense that the algorithm does not depend on the details of the imaging problem[8]. The algorithm is presented in Fig. 4. T and

E represent the annealing temperature and entropy of the system at some instance i, ΔE is the energy gap or corresponding change in entropy resulting from perturbation δ. SR provides a mechanism for uphill climbing the probability for this climb is given by the Boltzmann probability function:

$$p = e^{-\Delta E / T}$$

As T is gradually relaxed, the system is less likely to accept uphill moves in latter stages. For optimum control of T, we used the following exponential annealing schedule[32] with $0.77 \leq \alpha \leq .99$

$$T_{i+1} = \alpha T_i$$

With each annealing cycle, a small random perturbation,δ is added to each parameter, the value of which is defined as the product of a random variable $q \in [-0.5,0.5]$ and some stochastic value between [0,1]. SR mutation is applied only once every generation.

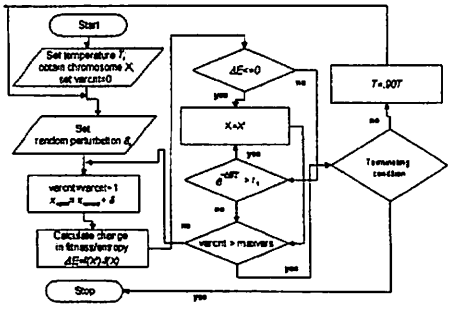

Fig. 4 Stochastic relaxation

In integrating the abovementioned operators to EA, the hybrid model in Fig 5 is employed. Per this model, three sets of individuals comprise the new population[12,13,14]. The first group consists top-ranking individuals (elites) from the previous generation that are translated without changes to the new generation[16]. The second set is made up of individuals resulting from a special local operator(*Concurrent Simplex*) applied to top members of the previous generation. Last is the set created through conventional EA crossover and mutation.

The model, originally developed by Yen et al for Genetic Algorithms, used simple operators and applied a concurrent probabilistic simplex operator on top ranking individuals. The control structure and operators have been improved in the proposed method without compromising the original's strengths. The algorithms and operators are shown in Fig. 6.

For each generation, the EA generates a highly competitive population of individuals. Only the best individuals from each operations are chosen to form the new population; resulting in dramatic increase in convergence.

For coventional EA reproduction, a multi-parent Simplex-based (SPX) operator with Boundary-Extension by Mirroring (BEM) is used[17]. Proposed by Tsuitsui et al, SPX works by uniformly picking N vector values from an expanded simplex generated by N parents. In this case, we set the number of parents is equal to the number of parameters to be optimized. BEM is a supporting algorithm developed to facilitate SPX and other multi-parent algorithms' location of optimum situated near the corner of the search space. Functional values of points outside the boundary are computed as though they belong inside the search space at points symmetrical to the boundary. An extension coefficient, r_e is introduced to attenuate the boundary by a factor of $1 - r_e$ in each dimension.

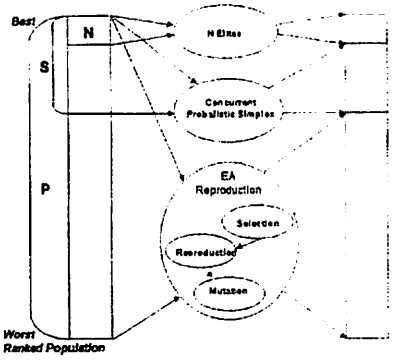

Fig. 5 Hybrid EA Architecture

SPX with BEM is reputed to work well with functions having multi-modality and epistasis. Nonetheless, convergence is slow as the MNT (i.e. mean number of function evaluations where the optimum is reached) is noticeably large, generally running to thousands. This was improved through hybridization.

Yen's GA Simplex Algorithm	EA Simplex Algorithm	Hybrid EA Operators
(Initialize) Generate a random population of size P Repeat • (Evaluate and Ranking) Evaluate the fitness of each chromosome. Rank them based on fitness results • (N Elites) Copy N elites to the next generation • (Simplex) Apply probabilistic simplex to the top S-N chromosomes and copy generated chromosomes to the next generation • (Selection) Select P-S chromosomes based on ranking or fitness and copy to the next generation • (Mutation) Apply mutation with the mutation probability to the P-S chromosomes • (Crossover) Apply 2 parent crossover with the crossover probability to the P-S chromosomes Until a termination condition is set	(Initialize) Generate a random population of size P Repeat • (Evaluate and Ranking) Evaluate the fitness of each chromosome. Rank them based on fitness results • (N Elites) Move N elites from old to the next generation • (Selection) Select a separate P chromosomes from old generation via roulette wheel for reproduction • (Crossover) Apply multi-parent reproduction with the crossover probability to the P chromosomes • (Selection) Select P-S best chromosomes from P and transfer to next generation • (Simplex) Apply stochastic simplex to the top S chromosomes of the old generation and copy the best S-N chromosomes to the next generation • (Mutation) Apply SR mutation with the mutation probability to the new population chromosomes Until a termination condition is set	Crossover operator simplex parent N+1 parent Reproduction operator (SPX) Multi-parent crossover (MPC) Mutation operator Stochastic ... mutation ... algorithm ... temperature ... (SRM) Selection Scheme Elitist roulette wheel selection scheme Hybrid Operator Concurrent Stochastic Simplex Other operator Evolutionary operator by Mirroring (EBM)

Fig. 6 Algorithms and Operators

The integration of all these operators produced an EA that has SPX's ability to handle epistasis, Stochastic Relaxation and Simplex' ability for local tuning and EA's global search ability. Lastly, MPC (Multi-point Crossover) was also developed for swapping parental sections at randomly selected points. The tri-hybrid method was used successfully in overlapping signal resolution.

4.2 *Superresolving EA Hybrid*

A flowchart of the superresolving multi-parent EA hybrid algorithm utilizing the cost function discussed in section 3 is

shown.

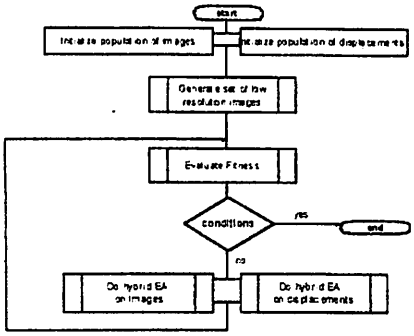

Fig. 7 Flowchart of superresolving EA hybrid

Two sets of populations representing the estimates for displacements and high resolution image respectively are maintained. Disjoint EA operations are applied to each. Low resolution frames are generated for each pair of individuals. The fitness for each pair is calculated by comparing the calculated and observed low resolution frames using the fitness function in section 3. An individual's final fitness will be the best fitness value taken over all pairings with the opposite set. This is generalized below:

$$E(ind_{i,}) = \min\lfloor E(i,1), E(i,2), E(i,3)...E(i, popsize_2)\rfloor$$

The optimum solution can be obtained by minimizing the costs of both unknowns. Acceptable results can be obtained in as little as 10 generations.

Another interesting feature is, that unlike other methods, where the relative displacements are determined at the low resolution image level, we have been moved the estimation up to the source image level. By having only to estimate the number of whole pixel shifts in the high-resolution image, the search space is reduced from real to whole integers. Initializing a portion of the initial population with interpolated low-resolution images also facilitated convergence.

Lastly, computer simulation results illustrate the effectiveness of the procedure even for frames corrupted with Gaussian noise.

5 Experiment and Results

We carried out computer simulations to validate the applicability of our method for superresolution. A standard 64 x 64 Lena image was used for the experiment. The original image was sub-sampled to produce 4 (*32 x 32*) shifted low-resolution images. Separate experiments simulating noise-free and noisy conditions were conducted.

Population sizes of 20 and 30 were assigned for image and displacement estimates. Number of parents, crossover rate, mutation rate, number of elites and α were set at3, 80%, 1%, 5 and 0.0005 respectively.

The results of both experiments are shown in the accompanying sheets. Figure 8 shows the original and low-resolution image samples (both with and without noise). Figure 9 compares the bicubic and b-spline interpolation results, one obtained using a modified SR method and that of the hybrid EA. Detailed description of interpolation kernels is beyond the scope of this paper, but can these be found in several image processing literature[10].

To provide analytical support to visual evaluation of results, the Means Square Error (MSE) and Peak Signal to Noise Ratio (PSNR) were calculated. Line profiles (Fig. 10) and Fourier magnitude images (Fig.11 and Fig. 12) were likewise prepared.

$$MSE = \frac{\|original - estimated\|^2}{(xres * yres)}$$

$$PSNR = -10\log_{10}(MSE / 255^2)$$

It can be seen from the line-profile results that new high frequency details are introduced by the EA algorithm. Because interpolation methods work only within the confines of the given data, they are not capable of introducing new information.

The value of the regularization parameter is determined on a per experiment basis. A too large λ results in a blurred image, one too small, on the other hand, results in too many oscillations.

6 Conclusion and Future Work

A tri-hybrid EA approach to image superresolution has been proposed. This compact method has been shown to outperform conventional interpolation based methods. Its main merit lies in its ability to do both image registration and restoration in one operation.

Future work include testing the benefits of pre and post processing in improving overall image quality, determination of a way to set the regularization parameter adaptively and exploring the possibility of harnessing parallel processing as a means to simplify and speed up computation.

7 References

1. S.P. Kim, H.K. Bose, and H.M. Valenzuela "Recursive reconstruction of high resolution image from noisy undersampled frames" *IEEE Trans. Acoust., Speech, Signal Processing* **38**,1013-1027(1990.)
2. K. Aizawa, T. Komatsu, and T. Saito, " A Scheme for acquiring very high resolution images using multiple cameras," *Proc. 1992 Int. Conf. Acoust., Speech, Signal Processing* **3**, 289-292 (1992.)
3. J.H. Shin, J.H. Jung, and J.K. Paik, "Regularized iterative image interpolation and its application to spatially scalable coding," *IEEE Trans. Consumer Electronics* **44**, 1042-1047 (1998.)
4. T. Numnonda, M.Andrews, R. Kakarara, "High resolution image reconstruction by simulated annealing," *Optics Communications*, **108**, 24-30 (1994.)
5. N. Nguyen "Numerical techniques for image superresolution." *Ph.D. Thesis*, Stanford University (1999.)
6. N.K. Bose, K.J. Boo, "High resolution image reconstruction

with Multisensors," *Optics Communications*, **9**, 294-304 (1998.)
7. T. Ando, "Trend of high resolution and high-performance solid state imaging technology," *J. ITE Japan* **44**, 105-109 (1992.)
8. I.C. Busko, "Stochastic relaxation as a tool for bayesian modeling of astronomical images," *Astronomical Data Analysis Software and SystemsIV ASP Conference Series* 77, (1995.)
9. Y.W. Chen, Z. Nakao, K. Arakaki, X. Fang, and S. Tamura, "Restoration of gray images based on a genetic algorithm with Laplacian constraint," *Fuzzy Sets and Systems* **103**, 285-293 (1999.)
10. F. Candocia, "A unified superresolution approach for optical and synthetic aperture radar images", *Doctoral thesis*, Univ. Florida (1998.)
11. T.J. Connolly, and R.G. Lane, "Gradient Methods for Superresolution," *Proc. Int. Conf. On Image Processing* **1**, 917-920 (1997.)
12. N.E. Mendoza,Y. W. Chen, Z.Nakao, T.Adachi, and Y. Masuda, "A real multi-parent tri-hybrid evolutionary optimization method with applications in the resolution of overlapping signals," *Proc. IEEE Int. Conf. Industrial Control and Instrumentation*. 2837-2842 (2000.)
13. Yen, J. Liao, B. Lee, and D. Randolph, "A hybrid approach to modeling metabolic systems using a genetic algorithm and simplex method," *IEEE Transaction of Systems, Man and Cybernetics* **28(2)**, 173-189 (1998.)
14. J. Renders, and H. Bersini, "Hybridizing genetic algorithms with hill-climbing methods for global optimization:2 possible ways," *Proceedings of the 1st IEEE Conference on Evolutionary Computation*, 312-317 (1994.)
15. J.A. Nelder, and R. Mead, "A simplex method for function minimization," *Computer Journal*, 7, 308-313 (1965.)
16. Z. Michalewics, *Genetic Algorithm + Data Structures Evolution Programs* (Springer-Verlag, Berlin. 1992.)
17. S. Tsutsui and M. Yamamura, "Multi-parent recombination with simplex crossover in real coded genetic algorithms," *Proceedings of the GECCO '99* (1999.)

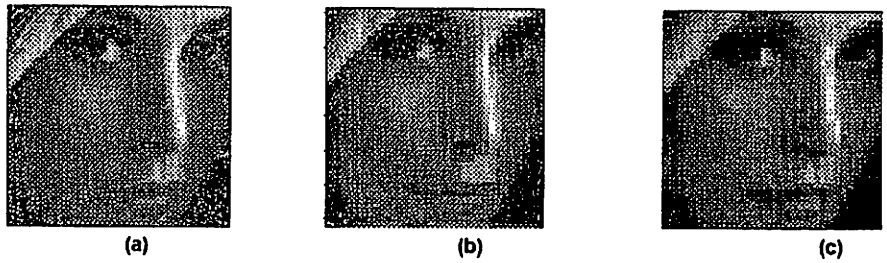

Fig. 8 Images used in the experiments; (a) original 64X64 high resolution image, (b) 32x32 shifted image without noise, (c) 32x32 shifted sub-sampled image with Gaussian noise

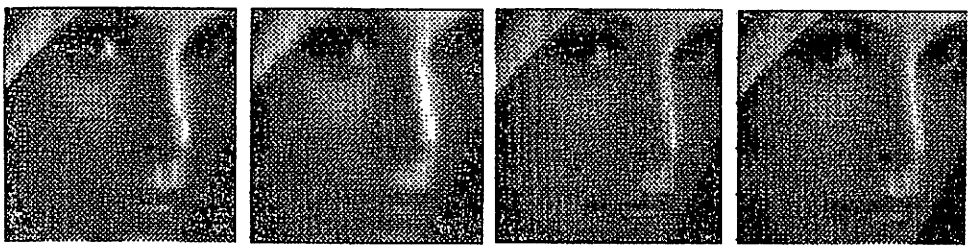

Fig. 9 *(a-d) show* results of 32x32 to 64x64 expansion using noise-free data. (d-h) show results from noisy frames.

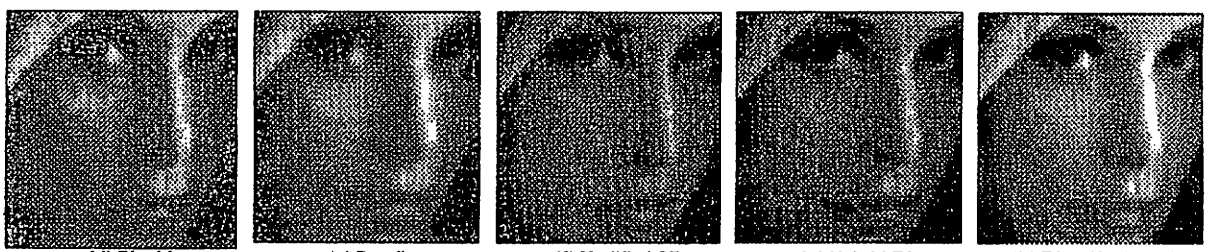

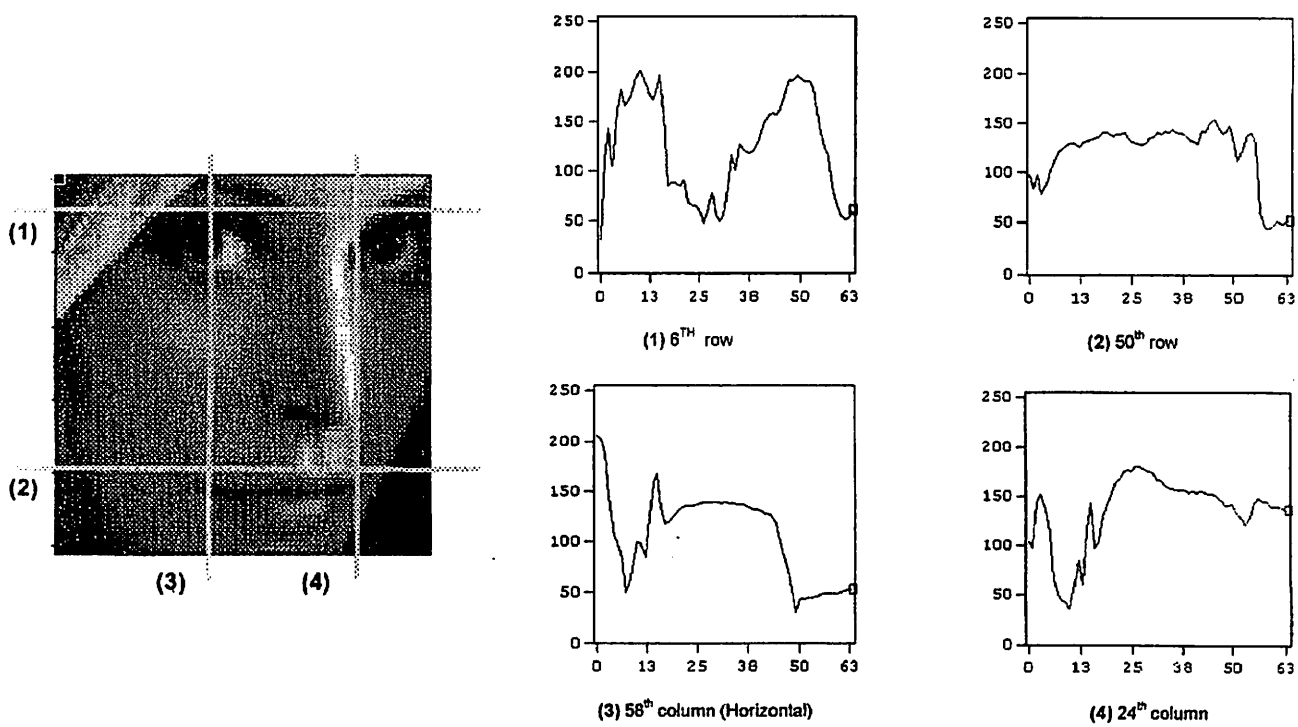

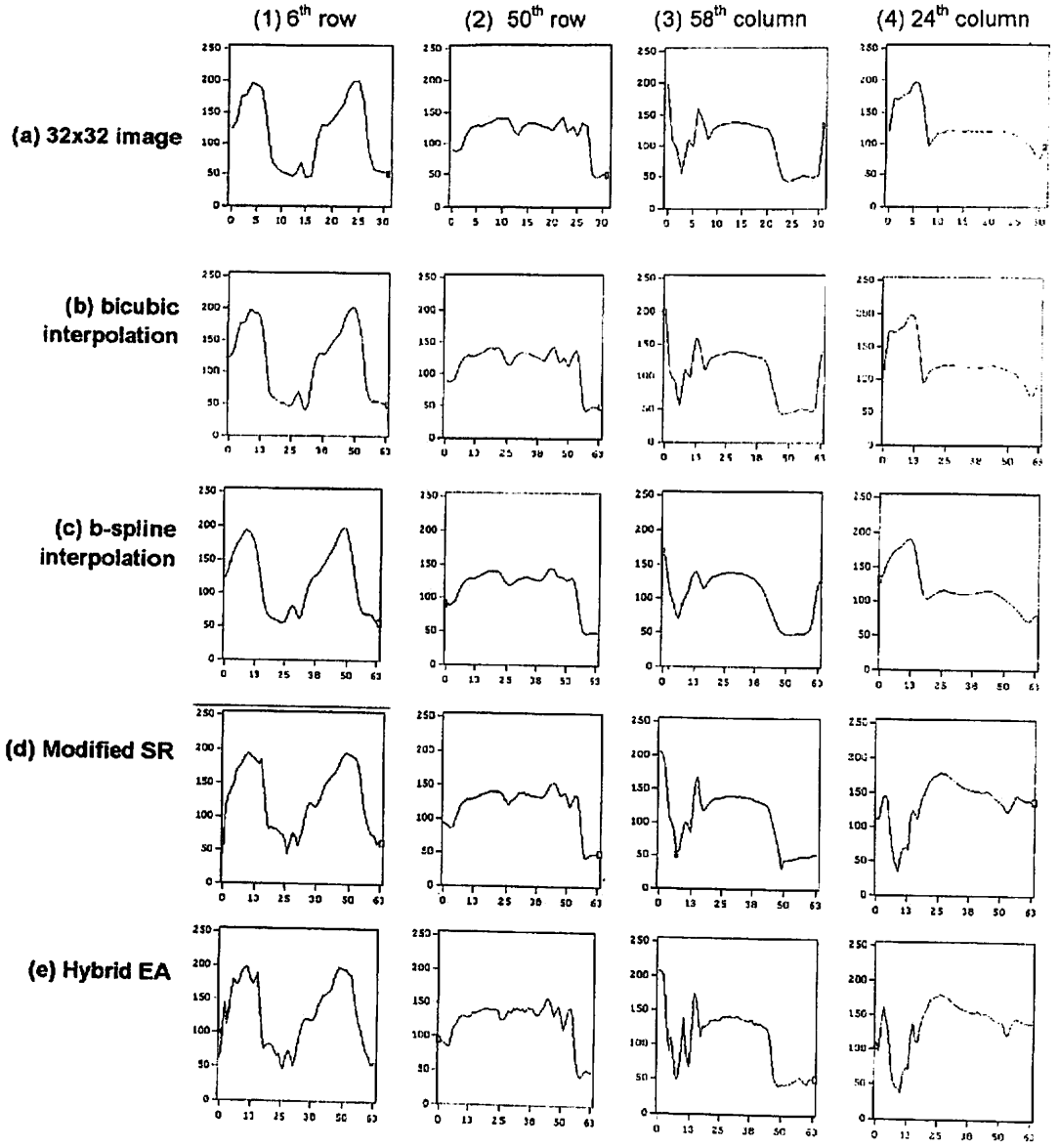

Fig. 10 The ideal line profiles are shown in 1-4. The line profile set of a 32x32 image is given in (a). Results for bicubic, b-spline, improved SR and hybrid EA are given in (b-e). Line profiles of SR and hybrid EA results using noisy are given below.

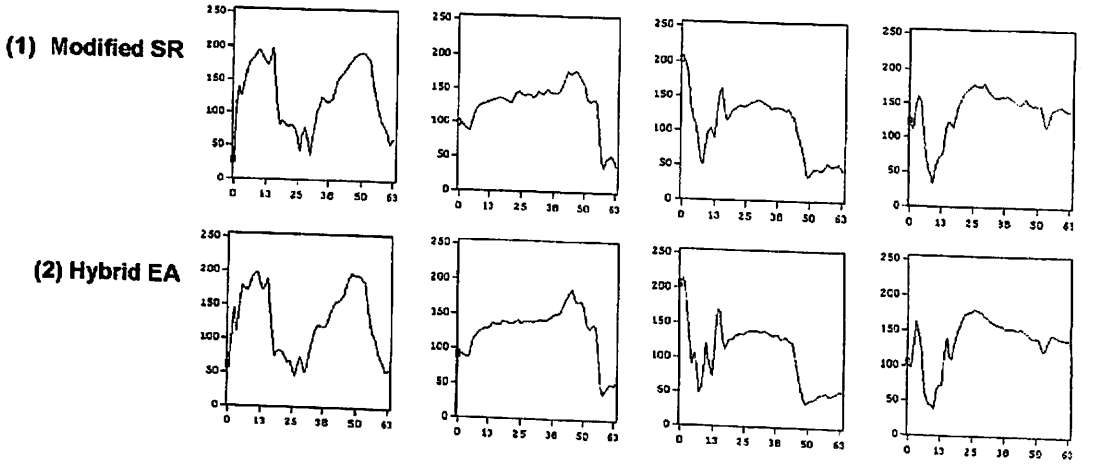

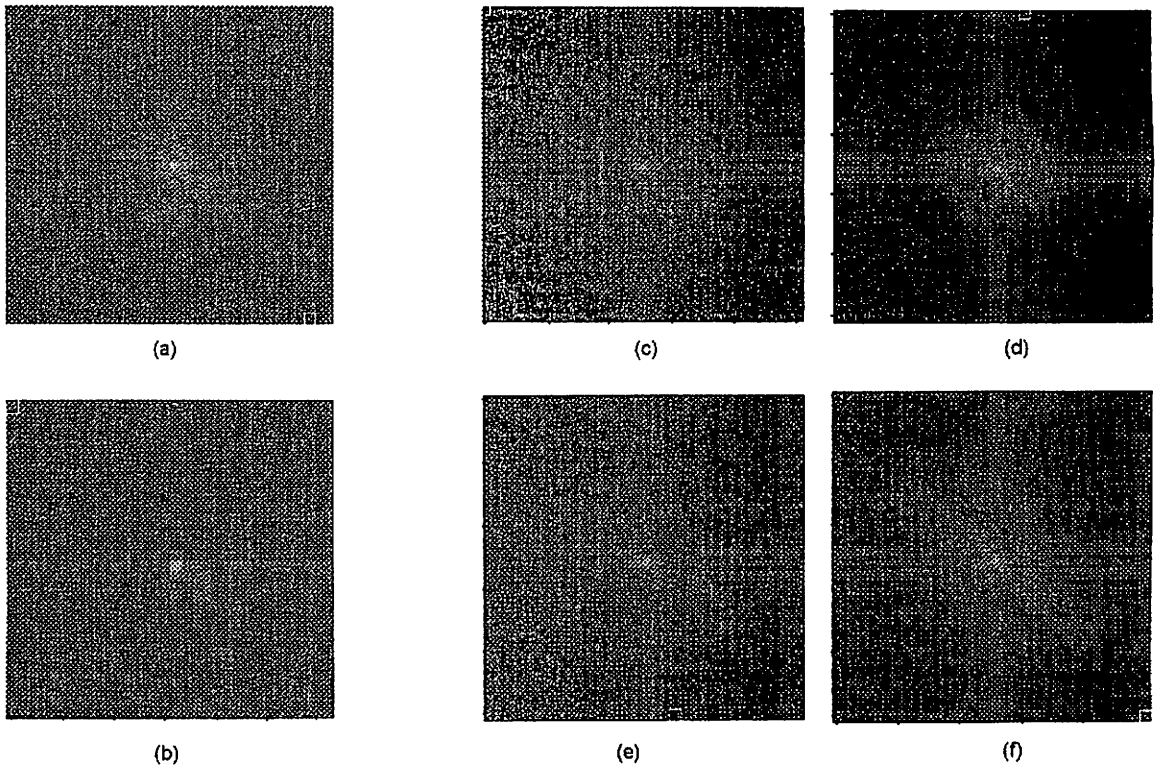

Fig. 11 Fourier magnitudes images of (a) original image (b) a low resolution frame (c) BC convolved image (d) B-spline interpolated image (e) SR and (f) hybrid EA results. Note the addition of high frequency components.

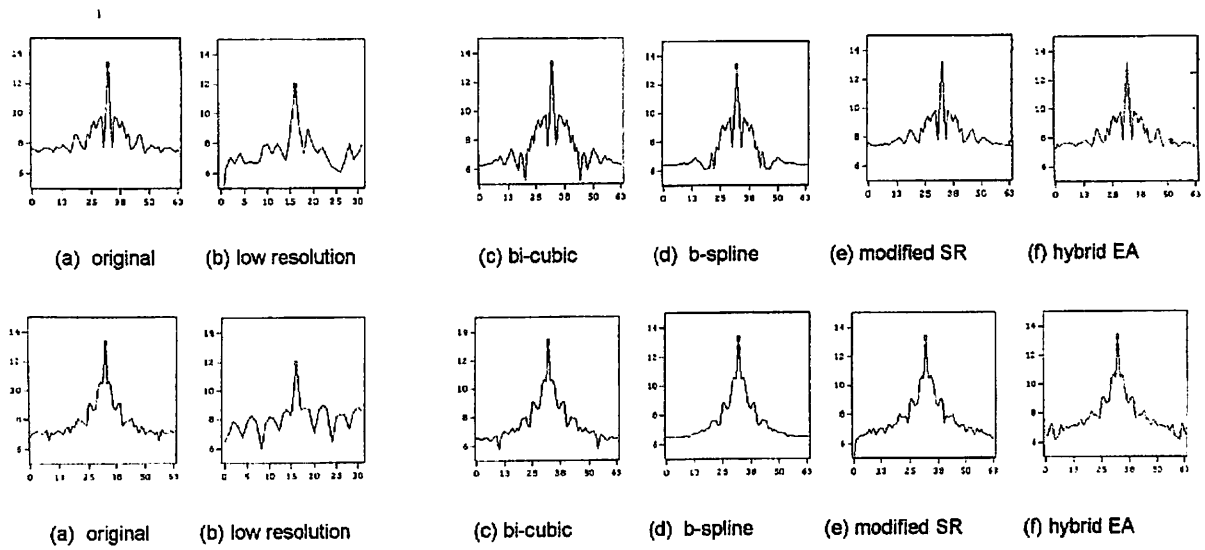

Fig. 12 Line profiles of Fig. 11 fourier images. Top and bottom rows show profiles for vertical and horizontal axes respectively.